Journal of Engineering Mathematics (2006) 55: 41–64
DOI 10.1007/s10665-005-9026-x

Approximate mathematical models in high-speed hydrodynamics

EMIL V. PARYSHEV
Central Aerohydrodynamic Institute named after Prof. N.E. Zhukovsky (TsAGI), Moscow Branch "Moscow Complex of TsAGI" 17, Ulitsa Radio, Moscow 105005, Russia (sparyshev@mail.ru)

Received 30 September 2003; accepted in revised form 14 November 2005 / Published online: 26 July 2006

Abstract. Approximate solutions of some problems in high-speed hydrodynamics are given, the solutions being based upon well-known approaches, such as the principle of independence of cavity expansion (Logvinovich), formulation of the problem of the immersion of a solid contour into liquid (Wagner), various models of cavity closure in its tail, etc. Theoretical studies of the dynamic properties of slender ventilated cavities are performed. The mathematical model of a cavity is obtained in the form of a system of nonlinear time-delay differential equations. The linear theory of cavity stability and oscillations is developed for various cavity types. The mechanism of nonlinear cavity oscillations accounting for gas-bubble detachment is considered, and the results of extensive numerical experimentation are presented. A theoretical model of cavity closure is proposed that develops the well-known Efros approach with a re-entrant jet. An approximate analysis of the model has been performed. A planar problem of the impact and immersion of an expanding cylinder into liquid with a cylindrical free surface of variable radius is solved in Wagner's formulation.

Key words: cavitation, dynamic stability, immersion into liquid, planing, pulsation

1. Introduction

Despite the tremendous progress of computational-fluid-dynamics (CFD) approaches in high-speed hydrodynamics, the methods based upon relatively simple physical considerations and approximate mathematical models are still of interest. These methods are widely used in such areas of hydrodynamics as supercavitation and those close to it like planing, immersion of bodies into liquid, and jet flows.

These methods include some prolific ideas such as the principle of independence of cavity expansion by Logvinovich [1, pp. 128–130], Wagner's formulation of the immersion of a solid contour into liquid [2], the plane-cross-sections method used in the theory of planing [3], various models of cavity closure in its tail including the well-known Efros approach with a re-entrant jet [4], etc.

Within these approaches, this paper addresses the following three independent issues related to supercavitaion:

- Research into the intrinsic properties of a ventilated cavity as a dynamic system (Section 2)
- Impact and immersion of a cylinder through a cylindrical liquid surface (Section 3)
- A theoretical model of cavity closure onto a liquid jet (Section 4).

Both scientific and applied aspects drive the interest in supercavitation. Cavitation-based technologies are used in various areas of R&D; some of these are described, *e.g.*, in the Proceedings of the International Summer Scientific School on High Speed Hydrodynamics held on June 16–23, 2002 in the city of Cheboksary, Russia. Among these areas are underwater vehicles moving in the supercavitation mode [5–8] and appropriate propulsors [9–10],

cavitation-free turbo-pumps for space-rocket engines [11], high-speed shipbuilding [12] and prevention of cavitation on propeller blades and rudders of ships [13], use of cavitation in manufacturing and operational processes in industry and transportation [14, 15].

Section 2 of this paper addresses the investigation of the intrinsic properties of a cavity as a dynamic system. This is one of the main parts of the whole problem of supercavitation. Many papers have focused on studies of these issues, including the known phenomenon of cavity oscillations [16–18].

The equation of cavity expansion plays a key part in cavity dynamics. For practical analysis, especially for unsteady cavities, the most effective are the methods based upon slender-body hydrodynamics and integral conservation laws, including the known theory of slender cavities. In the present paper the equation for a slender unsteady cavity as proposed by Logvinovich and Serebryakov [19, 20] is used; this equation expresses the known principle of independence of cavity expansion [1, pp. 128–130].

The equation makes it possible to write down a closed system of nonlinear time-delay differential equations describing variations of cavity geometry and internal pressure [21]. Relying upon the obtained system of equations, some unsteady cavitation problems have been solved [22–28]. The most comprehensive presentation of these results is in the author's paper [29].

A planar problem of impact and immersion of a cylinder through a cylindrical liquid surface will be considered in Section 3. Being valuable for their own sakes, problems of that kind are also used as constituent parts of the approximate method of planar cross-sections [3].

The problem of immersion of a cylinder in a fluid through a horizontal free surface at small submergence was considered by Logvinovich [1, pp. 72, 79–80] in Wagner's formulation [2]. The solution for the problem of immersing a cylinder in a narrowing cylindrical cavity (for small gaps between the body and the cavity), as obtained by the author, was partially presented in the papers by Logvinovich [30, 31]. In more complete form, this solution was published in [32, 33], with an addition being made by Vasin for an arbitrary relationship between the radius of a body and that of the cavity.

The present paper contains additional material: *e.g.* the planar problem of the oblique impact of a circular arc, the problem being of interest in itself; cavity and cylinder expansion are considered apart from cavity narrowing; the hydrodynamic force acting on the cylinder is determined approximately within a shock-problem formulation. A more detailed consideration of the problem is given in [34].

A model of cavity closure onto a jet is considered in Section 4. The jet may appear due to some specific features of cavitation flow, *e.g.* gas injection in the case of a ventilated cavity.

There are many theoretical models describing cavity closure in its tail. The most well-known of these are described in [35, pp. 176–200]. First of all there is Kirchhoff's cavity at cavitation number $\sigma = 0$, where cavity boundaries go to infinity. For $\sigma > 0$, we can mention the model of Zhukovsky and Roshko with cavity closure onto solid plates, Ryaboushinsky's model with closure onto a solid body of special shape, Tulin's models with spiral vortices, Efros' model with a re-entrant jet and others.

In Section 4 a model of cavity closure onto a central liquid or incompressible gas jet is described and its approximate analysis given, the model being in some respects opposite to that of Efros [4]. A circular re-entrant jet formed from a central jet is considered in this model instead of the re-entrant jet formed from external flow in Efros' model.

2. The dynamic theory of supercavitation

2.1. The equation of cavity-cross-section expansion

The process of cross-section expansion for an axisymmetric cavity is described by the differential equation [19, 20]:

$$\frac{\partial^2 S(h,t)}{\partial t^2} = -\frac{k}{\rho}\Delta p(h,t) \tag{2.1}$$

in which h is a coordinate describing the cross-section on the cavitator trajectory, the coordinate being associated with quiescent liquid (see Figure 1, a cavitator is a moving body that produces an elongated cavity behind it), $k = k(\sigma)$ is a coefficient slightly affected by the cavitation number. (Note that the equation for the expansion of a planar cavity has a structure similar to (2.1); hence all the results below are applicable to planar cavities within the accuracy of constant parameters.)

If k is constant, the integral of Equation (2.1) is

$$S(h,t) = S_0 + S_0' V(t_h)(t - t_h) - \frac{k}{\rho}\int_{t_h}^{t}\int_{t_h}^{u}\Delta p(h,v)\mathrm{d}v\,\mathrm{d}u. \tag{2.2}$$

Here $S_0 = \pi R_n^2$ and $S_0' = S_0'(\sigma)$ is the initial rate of cavity expansion (a weak function of cavitation number), $t_h = t_h(h)$ indicates the time instant when the cavitator passes through coordinate h.

The coefficients of Equation (2.2) were calculated for various cavitators as $S_0'/2\pi R_n = f_1(\sigma)$, $k/4\pi = f_2(\sigma)$ (known approximations by Gouzevsky [36] for Ryaboushinsky's cavities have been used). For example, for $\sigma = 0{\cdot}02$ we have the following values for a disk: $f_1 = 0{\cdot}439$,

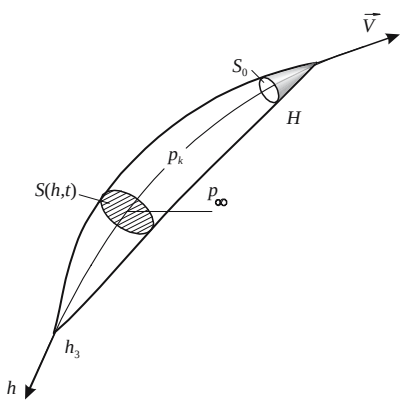

Figure 1. Supercavitation flow past a cavitator.

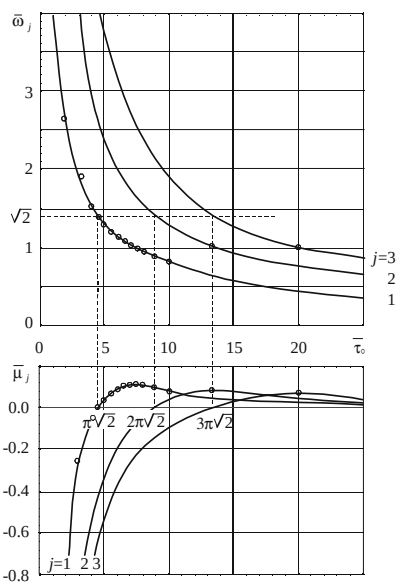

Figure 2. Root trajectories of the characteristic equation of cavity oscillation (real $\bar{\mu}_j(\bar{\tau}_0)$ and imaginary $\bar{\omega}_j(\bar{\tau}_0)$ parts of eigenvalues versus the dimensionless time lag).

and $f_2 = 0{\cdot}219$. Actually, the dependence of the functions f_1 and f_2 on σ does not greatly affect the size of the cavity mid-section. Note that the coefficient $f_2(\sigma)$, which governs the law of cross-section narrowing, is practically the same for all types of cavitators.

2.2. Closed problem formulation

A cavity is regarded as a variable-volume gas-filled space with gas injection and losses. Equation (2.2) must be completed with the following:

(i) Expression of the gas volume

$$Q(t) = \int_{H(t)}^{h_3(t)} [S(h,t) - S_T(h,t)]\,\mathrm{d}h \tag{2.3}$$

in which S_T is the cross-sectional area of a body inside the cavity, H is the cavity inception coordinate, h_3 is the coordinate of the section in which the cavity is closed (Figure 1);

(ii) Equation for the gas mass balance inside the cavity

$$\frac{\mathrm{d}}{\mathrm{d}t}(Q\rho_k) = \dot{m}_n - \dot{m}_y, \quad \rho_k = \rho_k(p_k) \tag{2.4}$$

in which ρ_k is the gas density in the cavity (constant throughout the whole volume; no wave processes in the gas are considered), $\dot{m}_n, \dot{m}_y$ are mass rates per second for gas injection and loss;

(iii) Equation for cavitator motion

$$\frac{\mathrm{d}\mathbf{V}}{\mathrm{d}t} = \mathbf{F}(V, H, h_3, p_\infty, p_k, \ldots). \tag{2.5}$$

2.3. Time-delay differential equations

The integro-differential system (2.2–2.5), which does not have any regular methods of solution apart from numerical analysis at discrete sections, is transformed into the system (2.6) of nonlinear time-delay differential equations, the time lag being variable. The main idea of the transformation is to exclude integral relations by means of differentiating them with respect to a parameter (the time in this particular case).

$$\ddot{Q} = -\frac{k}{\rho}\int_H^{h_3} p_\infty(h,t)\,\mathrm{d}h + \frac{k}{\rho}p_k(t)l + \dot{h}_3\frac{\partial S(h_3,t)}{\partial t} + S_0'V^2 - \dot{V}[S_T(l) - S_0] - VS_T'(l)\dot{l},$$

$$\dot{h}_3 = -\frac{\partial S(h_3,t)/\partial t - VS_T'(l)}{\partial S(h_3,t)/\partial h - S_T'(l)}, \quad \dot{l} = \dot{h}_3 + V, \quad l = h_3 - H, \quad \dot{H} = -V \quad \dot{\tau} = 1 + \frac{\dot{h}_3}{V(t-\tau)},$$

$$\frac{\mathrm{d}}{\mathrm{d}t}\frac{\partial S(h_3,t)}{\partial t} = -\left\{\frac{S_0'\dot{V}(t-\tau)}{V(t-\tau)} + \frac{k}{\rho}\left[\frac{\Delta p(h_3,t-\tau)}{V(t-\tau)} + \int_{t-\tau}^{t}\frac{\partial p_\infty(h_3,v)}{\partial h}\,\mathrm{d}v\right]\right\}\dot{h}_3 - \frac{k}{\rho}\Delta p(h_3,t),$$

$$\frac{\partial S(h_3,t)}{\partial t} = S_0'V(t-\tau) - \frac{k}{\rho}\int_{t-\tau}^{t}\Delta p(h_3,v)\,\mathrm{d}v, \tag{2.6}$$

$$\frac{\partial S(h_3,t)}{\partial h} = S_0'\left[1 - \frac{\dot{V}(t-\tau)\tau}{V(t-\tau)}\right] - \frac{k}{\rho}\left[\frac{\Delta p(h_3,t-\tau)\tau}{V(t-\tau)} + \int_{t-\tau}^{t}\int_{t-\tau}^{u}\frac{\partial p_\infty(h_3,v)}{\partial h}\,\mathrm{d}v\,\mathrm{d}u\right],$$

$$\Delta p(h,t) = p_\infty(h,t) - p_k(t), \quad S_T = S_T(x).$$

Here l is the cavity length, $x = h - H$ is the distance between the cavitator and the given cross-section, $t - \tau$ is the moment at which the cavitator passes through coordinate h_3, τ is a

time lag. The assumption is made that the gas pressure inside the cavity is almost constant lengthwise and depends only upon time [16].

Equations (2.6) are completed with the differential equation for the gas pressure

$$\dot{p}_k = \frac{\dot{m}_n - \dot{m}_y - C\dot{Q}p_k^n}{nCQp_k^{n-1}}. \tag{2.7}$$

This is derived from (2.4) assuming that gas density and pressure conform to the polytropic equation $\rho_k = Cp_k^n$, in which $1/n$ is a polytropic factor. Here we use known data on gas withdrawal along trailing vortices [37, 38], and under conditions close to vapour cavitation [1, p. 146], as well as a model of withdrawal due to gas-jet ejection. The gas withdrawal in the form of periodical detachment of bubbles, which was observed in experiments conducted by Michel [16] and others, is realized during numerical modeling of cavity pulsations [26] due to periodical pinching and detachment of the cavity tail part (see Figure 10).

2.4. Linear theory of cavity stability and oscillations (basic problem)

2.4.1. *Problem formulation*

The simplest cavitation flow under steady input conditions, namely an axisymmetric cavity in a weightless liquid ($p_\infty = \text{const}$) at constant cavitator velocity V and constant gas mass in the cavity ($Qp_k^n = \text{const}$) is considered. The equations of cavity dynamics (2.6) and (2.7), after linearization, produce an equation for small pressure oscillations:

$$p_k'''(\bar{t}) + p_k'(\bar{t}) + p_k'(\bar{t} - \bar{\tau}_0) - \frac{2}{\bar{\tau}_0}p_k(\bar{t}) + \frac{2}{\bar{\tau}_0}p_k(\bar{t} - \bar{\tau}_0) = 0. \tag{2.8}$$

Here $T = \sqrt{n\rho Q_0/(kl_0 p_{k0})}$ is a time scale, $\bar{t} = t/T$ is a dimensionless time, $p_{k0}, Q_0, l_0, \tau_0 = l_0/V$ are steady parameter values. The sign $'$ denotes derivatives with respect to $\bar{t}$. Equation (2.8) and the total problem have only one governing parameter, *i.e.*, the dimensionless time lag $\bar{\tau}_0 = \tau_0/T$. Approximating the cavity shape by an ellipsoid of evolution will produce:

$$\bar{\tau}_0 = \sqrt{\frac{12}{n}\cdot\frac{p_{k0}}{p_\infty - p_{k0}}} = \sqrt{\frac{12}{n}\left(\frac{\mathrm{Eu}}{\sigma} - 1\right)}. \tag{2.9}$$

2.4.2. *Characteristic equation and eigenvalues*

The time-delay Equation (2.8) belongs to the class of differential equations with a divergent argument, which are associated with great mathematical difficulties regarding their analysis. Equation (2.8) leads to the following transcendental characteristic equation

$$\bar{\lambda}^3 + \bar{\lambda} + \bar{\lambda}\mathrm{e}^{-\bar{\lambda}\bar{\tau}_0} - \frac{2}{\bar{\tau}_0} + \frac{2}{\bar{\tau}_0}\mathrm{e}^{-\bar{\lambda}\bar{\tau}_0} = 0 \tag{2.10}$$

with an infinite set of eigenvalues (roots). A method for solving such equations has been developed based on the numerical analysis of complex eigenvalues trajectories depending on one or several parameters; this method makes it possible to determine a root of any given number [22].

The essence of the method is as follows. When $\bar{\tau}_0 = \pi\, j\sqrt{2} \quad (j = 1, 2, \ldots)$, Equation (2.10) has purely imaginary eigenvalues $\bar{\lambda}_j = \mathrm{i}\bar{\omega}_j, \bar{\omega}_j = \sqrt{2}$. By differentiating (2.10) with respect to $\bar{\tau}_0$, we find

$$\frac{\mathrm{d}\bar{\lambda}}{\mathrm{d}\bar{\tau}_0} = -\frac{1}{\bar{\tau}_0^2}\frac{2 - \exp(-\bar{\lambda}\bar{\tau}_0)\,(\bar{\lambda}^2\bar{\tau}_0^2 + 2\bar{\lambda}\bar{\tau}_0 + 2)}{3\bar{\lambda}^2 + 1 - \exp(-\bar{\lambda}\bar{\tau}_0)\,(\bar{\lambda}\bar{\tau}_0 + 1)},$$

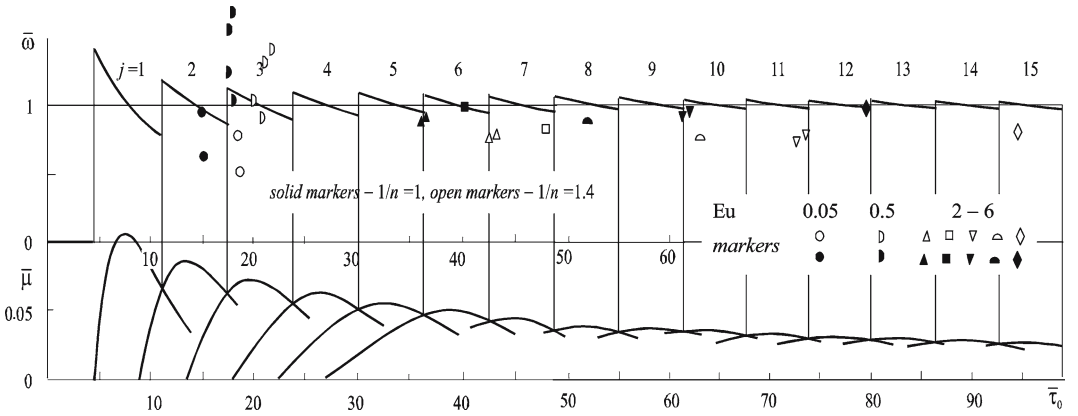

Figure 3. The dimensionless frequency of cavity oscillation as a function of the dimensionless time lag $\bar{\omega}_j(\bar{\tau}_0)$.

which is equivalent to two equations in terms of real variables:

$$\frac{\mathrm{d}\bar{\mu}}{\mathrm{d}\bar{\tau}_0} = -\frac{1}{\bar{\tau}_0^2}\frac{AC+BD}{C^2+D^2}, \quad \frac{\mathrm{d}\bar{\omega}}{\mathrm{d}\bar{\tau}_0} = -\frac{1}{\bar{\tau}_0^2}\frac{BC-AD}{C^2+D^2},$$

where A, B, C and D are appropriate functions of $\bar{\tau}_0, \bar{\mu}$ и $\bar{\omega}$. These equations are integrated numerically with initial conditions

$$\bar{\tau}_{0j} = \pi\, j\sqrt{2}, \quad \bar{\mu}(\bar{\tau}_{0j}) = 0, \quad \bar{\omega}(\bar{\tau}_{0j}) = \sqrt{2}.$$

Thus, the total system of eigenvalues of Equation (2.10) is determined, which includes a zero root of the third order and an infinite set of complex eigenvalues

$$\bar{\lambda}_j(\bar{\tau}_0) = \bar{\mu}_j(\bar{\tau}_0) \pm \mathrm{i}\bar{\omega}_j(\bar{\tau}_0), \quad j = 1, 2, \ldots, \quad 0 \le \bar{\tau}_0 < \infty.$$

Note that the third-order zero root may cause extraneous solutions like $c_1 + c_2 t + c_3 t^2$ if the accuracy of the numerical integration of (2.8) is not sufficient.

2.4.3. *Examination of the system of eigenvalues*

The obtained system of eigenvalues has a very well-defined structure, which makes it possible to find out the main cavity-dynamics properties. The trajectories of the first three roots of Equation (2.10) are illustrated in Figure 2. The dimensionless circular frequency $\bar{\omega}_j(\bar{\tau}_0)$ forms a family of monotonically decreasing functions. The real parts of the eigenvalues $\bar{\mu}_j(\bar{\tau}_0)$ are mutually intersecting functions of similar type that intersect the horizontal axis at the points $\bar{\tau}_0 = \pi j\sqrt{2}$. To the left of such a point, $\bar{\mu}_j < 0$, *i.e.*, the jth eigenvalue is stable. To the right of this point $\bar{\mu}_j > 0$, *i.e.*, the eigenvalue is oscillatory unstable. The situation is the same for any j.

The curves $\bar{\mu}_j(\bar{\tau}_0)$ show that a cavity is asymptotically stable for $\bar{\tau}_0 < \pi\sqrt{2}$, and oscillatory unstable for all $\bar{\tau}_0 > \pi\sqrt{2}$, the value $\bar{\tau}_0 = \pi\sqrt{2}$ (Eu/σ = 2·64) being a stability boundary. The instability of a linear system transforms in real nonlinear systems (to which a cavity may be referred) into self-excited oscillations (cavity pulsations) with finite amplitude and with a frequency equal or close to that of the linear system. The main nonlinear factor in the case of a cavity is the detachment of gas bubbles caused by the pinching of the cavity tail part by traveling waves.

The cavity oscillation frequency is determined by the physically meaningful root which has the greatest real part among all the other unstable roots for given $\bar{\tau}_0$. Thus, the dimensionless

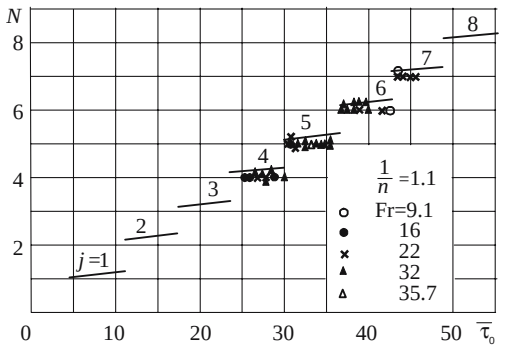

Figure 4. The number of waves along the cavity versus the dimensionless time lag.

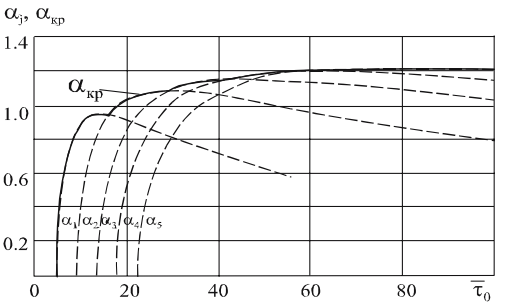

Figure 5. Stability boundaries for separate eigenvalues and the common envelope for cavity stability in terms of the damping coefficient.

frequency of asymptotic oscillations (actually the frequency of self-oscillations) is a saw-tooth function of $\bar{\tau}_0$ (Figure 3) consisting of portions of the consequent curves $\bar{\omega}_j(\bar{\tau}_0)$. The greater the value of $\bar{\tau}_0$, the smaller the tooth height; also $\bar{\omega} \approx 1$ for increasing values of $\bar{\tau}_0$. The "tooth spacing" appears to be 2π.

The dimensional circular frequency of oscillations is given by

$$\omega = \bar{\omega}/T = \bar{\omega}\sqrt{kp_{k0}l_0/(nQ_0\rho)}. \tag{2.11}$$

If $\bar{\tau}_0$ is large enough, then $\bar{\omega} \approx 1$ and ω is proportional to $\sqrt{p_{k0}}$.

Pressure oscillations inside a cavity are accompanied by waves on the cavity surface with wavelength $l_b = 2\pi V/\omega$. The number of waves along the length of the cavity is $N = l_0/l_b = \bar{\omega}\bar{\tau}_0/(2\pi)$. The function $N(\bar{\tau}_0)$ calculated with the use of the "saw" in Figure 3 is shown in Figure 4. This is also a discontinuous function. The number of waves along the cavity is close to an integer value equal to the number j of the dominating root. In the points of discontinuity, N increases step-wise by ~ 1. There is a simple estimate for $\bar{\omega} \approx 1$: $N \approx \dfrac{\bar{\tau}_0}{2\pi} = \dfrac{1}{\pi}\sqrt{\dfrac{3}{n}\left(\dfrac{\mathrm{Eu}}{\sigma} - 1\right)}$.

2.4.4. *The major physical conclusions*

- The similarity parameter for unsteady ventilated cavities is $\bar{\tau}_0 = \sqrt{\dfrac{12}{n}\left(\dfrac{\mathrm{Eu}}{\sigma} - 1\right)}$.
- The generic property of ventilated cavities under various conditions is their oscillatory instability, which causes the phenomenon of pulsation (self-oscillations) of cavities.
- The number of waves along an oscillating cavity changes stepwise by 1 (change of oscillation mode) under continuous variation of flow parameters (continuous variation of $\bar{\tau}_0$).

2.5. Comparison with experiments

The present theory clearly explains the most typical features of cavity oscillations, both in axisymmetric and planar cases. The results of numerous experiments and their detailed examination for oscillations of planar cavities past a wedge are presented in [16]. A detailed comparison [22] shows that, generally, the features described in that paper are quite close to those given by the present theory.

Theory and experiment for axisymmetric cavities past disks have been compared on the basis of multiple experimental data by different authors, the data varying greatly in terms of test conditions ($10 \le \mathrm{Fr} \le 120$, $0{\cdot}02 \le \sigma$, $0{\cdot}04 \le \mathrm{Eu} \le 10$). Some experimental data reduced to the form $\bar{\omega}(\bar{\tau}_0)$ are plotted as point marks over the theoretical graph in Figure 3. The experiments for $\mathrm{Eu} = 0{\cdot}05$ and $\mathrm{Eu} = 0{\cdot}5 (\bar{\tau}_0 \approx 20)$ were conducted in an open natural reservoir and were not intended specifically for investigation of oscillations, which is why some points exhibit scattering. Experiments for $\mathrm{Eu} = 2$–6 were done in a water tank specially made for the purpose of pulsation studies. The positions of point marks on the theoretical plot depend on the value of $1/n$. Solid points are related to $1/n = 1$ (isothermal process in gas), open points are for $1/n = 1{\cdot}4$ (adiabatic process). Comparing positions of solid and light markers of the same shape, one can see that a better match between test and theory is obtained for $1/n = 1$. The most typical from this point of view is one of the experimental cavities involving 12 waves. The appropriate point in Figure 3 lies within a 12-wave zone at $1/n = 1$ and within a 15-wave zone for $1/n = 1{\cdot}4$.

Stepwise pulsation-mode change is a subject of comparison between the theory and the experiments of Epshteyn on oscillations of horizontal disk-induced cavities (see Figure 4). The number of waves along the cavity are plotted by point marks as a function of $\bar{\tau}_0$ together with a theoretical step-like dependence $N(\bar{\tau}_0)$. Using different polytropic factors $1/n$ shows that the best agreement between theory and experiment is for $1/n = 1{\cdot}1$, *i.e.*, the process is close to isothermal.

2.6. Development of the linear theory

The method developed made it possible to solve some other problems of unsteady cavitation in a linear formulation.

2.6.1. *Vertical cavities in a gravity field*

Dynamic properties of vertical cavities in a liquid have been investigated for the case where gravity cannot be neglected. The peculiarity of such cavities is the vertical gradient of the external pressure. Vertical cavities have the same dynamic properties as those in a weightless liquid. The parameter $\bar{\tau}_0$ for vertical cavities is determined on the basis of the external pressure $p_\infty(h)$ being taken halfway the cavity length.

2.6.2. *Cavities with loss of gas*

Another issue of great interest is gas loss from a cavity and its effect on the cavity itself. The cavity model with constant gas mass inside (Section 2.4) leads to the conclusion that a cavity is always unstable if $\bar{\tau}_0 \ge \pi\sqrt{2}$. Meanwhile experiments in a test tank ($\bar{\tau}_0 \approx 20$–60) show that horizontal cavities may be both stable and oscillating, and usually it is an increase of gas injection that stops the oscillations.

Let us consider a cavity model with gas loss taken into account, the loss amount being a monotonically increasing function of gas pressure (that is, a monotonically decreasing function of the cavitation number σ): $\dot{m}_y = \dot{m}_y(p_k)$, $\partial \dot{m}_y / \partial p_k > 0$. In this case, the equation of small cavity oscillations is:

$$p_k'''(\bar{t}) + \alpha\, p_k''(\bar{t}) + p_k'(\bar{t}) + p_k'(\bar{t} - \bar{\tau}_0) - \frac{2}{\bar{\tau}_0} p_k(\bar{t}) + \frac{2}{\bar{\tau}_0} p_k(\bar{t} - \bar{\tau}_0) = 0. \tag{2.12}$$

The equation features an additional damping term $\alpha p_k''$, with

$$\alpha = \frac{\mathrm{d}\dot{m}_y / \mathrm{d}p_k}{C p_{k0}^n} \sqrt{\frac{\rho\, p_{k0}}{n k l_0 Q_0}}. \tag{2.13}$$

Considering the eigenvalues of the characteristic equation, one finds the general stability boundary $\alpha_{\kappa p}(\bar{\tau}_0)$ for the cavity (solid curve in Figure 5). The stability boundaries for separate eigenvalues $\alpha_j(\bar{\tau}_0)$ are shown as dashed lines in Figure 5. The cavity is stable for $\alpha > \alpha_{\kappa p}$. The appearance of $\alpha\, p_k''$ does not significantly affect the frequency values.

In the case of gas withdrawal from horizontal cavities along trailing vortices, let us use Epshteyn's formula [38]

$$\bar{Q}_y = \frac{Q_y}{Vd^2} = \frac{0{\cdot}42c_{x0}^2}{\sigma(\sigma^3 \mathrm{Fr}^4 - 2{\cdot}5c_{x0})},$$

where Q_y is volume per second rate of gas withdrawal from the cavity. The rate of gas loss is $\dot{m}_y = Cp_k^n Vd^2 \bar{Q}_y$. By differentiating this expression with respect to p_k and substituting the derivative in (2.13), we obtain the coefficient α as

$$\alpha = \frac{6}{\pi(1+\sigma)\bar{\tau}_0} \frac{\bar{Q}_y\sigma}{c_{x0}} \left(1 + \frac{\bar{\tau}_0^2}{3} + 1{\cdot}5\bar{\tau}_0^2 \frac{\bar{Q}_y\sigma}{c_{x0}}\right). \tag{2.14}$$

There is a complicated expression for $\bar{Q}_y\sigma/c_{x0}$ considered as a stability criterion for weight-affected cavities. The damping coefficient α grows as $\bar{Q}_y\sigma/c_{x0}$ increases. Substituting $\alpha = \alpha_{\kappa p}(\bar{\tau}_0)$ in the equivalence (2.14), we find the value of $\bar{Q}_y\sigma/c_{x0}$ corresponding to the stability boundary:

$$\left(\frac{\bar{Q}_y\sigma}{c_{x0}}\right)_{\kappa p} = -\frac{3+\bar{\tau}_0^2}{9\bar{\tau}_0^2} + \sqrt{\left(\frac{3+\bar{\tau}_0^2}{9\bar{\tau}_0^2}\right)^2 + \frac{\pi(1+\sigma)\,\alpha_{\kappa p}(\bar{\tau}_0)}{9\bar{\tau}_0}}.$$

A part of the theoretical stability boundary in the coordinates $\bar{\tau}_0$, $\bar{Q}_y\sigma/c_{x0}$ is plotted in Figure 6 as a solid line. Experimental results by Epshteyn and Lapin are shown by point marks. Experimental and analytical results are in close agreement.

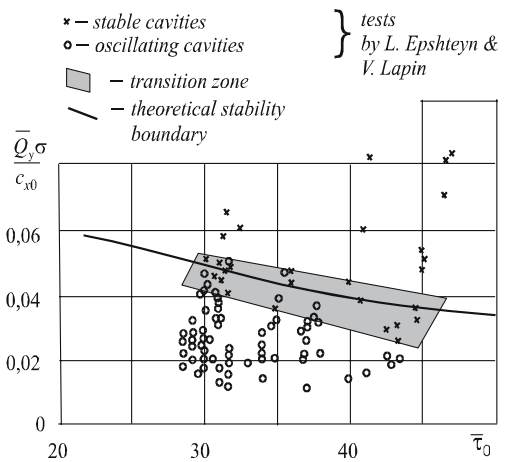

Figure 6. The cavity stability boundary in terms of dimensionless gas-injection rate.

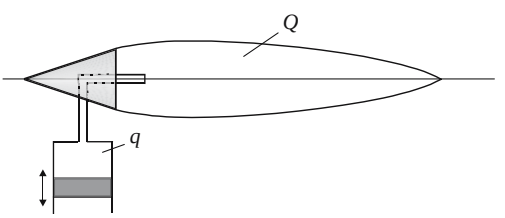

Figure 7. Excitation of the cavity oscillation.

2.6.3. *Jet-induced ejection of gas from a cavity*

The problem of a jet acting in the mode of gas ejection from a cavity has been considered. According to well-known ejection properties of turbulent jets, it is assumed that the ejection rate is proportional to the length of the part of the jet located inside the cavity. A survey of this model shows that the jet produces a small effect on cavity stability. The trail jet may dampen cavity oscillations within a limited parameter envelope, which corresponds approximately to the relationship $0{\cdot}8\text{–}0{\cdot}9 < \dfrac{\kappa R_0 V_0}{c_{x0} R_n V}\sqrt{\dfrac{\rho_0}{\rho_k}} < 1{\cdot}1\text{–}1{\cdot}2$. Here $\kappa = 0{\cdot}155$ is jet ejection coefficient; R_0, V_0, ρ_0 are radius, velocity and density of the jet; c_{x0}, R_n, V are cavitator drag coefficient, radius and velocity of the cavitator; ρ_k is gas density inside the cavity.

2.6.4. *Cavity forced oscillations*

It is interesting to study the reaction of a cavity as a dynamic system to an external disturbance. We will consider a method to excite cavity oscillations by means of a periodic variation of the volume q connected with the internal cavity volume Q (Figure 7). Wave processes in the gas are neglected; it is assumed that the total mass in the volume $Q+q$ is constant. After linearization, Equations (2.6) and (2.7) produce the equation for forced cavity oscillations

$$\bar{p}_k'''(\bar{t}) + \bar{p}_k'(\bar{t}) + \bar{p}_k'(\bar{t}-\bar{\tau}_0) - \frac{2}{\bar{\tau}_0}\bar{p}_k(\bar{t}) + \frac{2}{\bar{\tau}_0}\bar{p}_k(\bar{t}-\bar{\tau}_0) = -\bar{q}'''. \tag{2.15}$$

We denote a disturbance as $\bar{q} = \bar{A}e^{i\bar{\omega}\bar{t}}$ and pressure oscillations as $\bar{p}_k = \bar{B}e^{i\bar{\omega}\bar{t}}$. Equation (2.15) gives the amplitude and phase-frequency response functions $b = \left|\bar{B}/\bar{A}\right|$, $\arg\bar{B} = \pi + \varphi$, $\chi = \bar{\omega}\bar{\tau}_0/2$. The frequency-response functions of a stable cavity are shown in Figure 8 for $\bar{\tau}_0 = 3$. There is a resonance ($b > 1$) for $\chi \approx \pi$. As $\chi \to \infty$ $\varphi \to 0$, $b \to 1$, the cavity volume does not keep pace with the pressure disturbance at high frequencies, *i.e.*, the cavity becomes "rigid".

For unstable cavities, theoretically, there may be a method of external influence which would dampen cavity self-oscillations. Given the volume control law as $\bar{q} = \alpha \int \bar{p}_k d\bar{t}$, from (2.15) we will obtain Equation (2.12) considered above. A cavity is stable if $\alpha > \alpha_{kp}$ (Figure 5). For an unstable cavity with $\bar{\tau}_0 = 5$, we have the value $\alpha_{kp} = 0{\cdot}282$. Frequency-response functions in terms of amplitude for different values $\alpha > \alpha_{kp}$ are shown in Figure 9. The amplitude

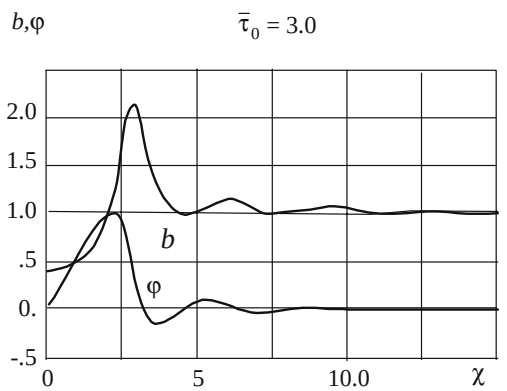

Figure 8. Frequency-response functions of a stable cavity.

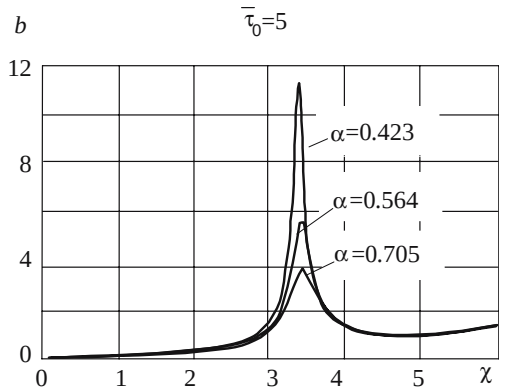

Figure 9. Frequency-response functions of an intrinsically unstable cavity with added artificial damping.

at resonance decreases if α increases. As can be seen from Figure 5, there is an estimate, namely $\alpha_{\mathrm{kp\,max}} \approx 1{\cdot}2$.

2.7. Nonlinear cavity oscillations with periodic detachment of gas bubbles

Along with a linear analysis, numerical integration of the full nonlinear system of the time-delay Equations (2.6, 2.7) has been performed with account taken for periodic detachment of gas bubbles. Let us use the following conditions: $V = \mathrm{const}$, $p_\infty = \mathrm{const}$, with gas injection rate $\dot{m}_n(t)$ and periodic bubbles detachment (other components of gas loss are neglected). Theoretically, waves on a cavity surface lead to instant cavity profile pinching and detachment of part of the volume (Figure 10); the said detached parts do exist in reality, though not so explicitly (*e.g.* [16]).

Note the qualitative peculiarities of nonlinear oscillations: not only do the cavity volume and length change stepwise at the moment of detachment, but the derivatives $\dot{Q}$ and $\dot{p}_k$ do so as well. Thus, this moment requires redefining the initial conditions. At the moment of bubble detachment, the cavity length features an infinite (though integrable) variation rate $\dot{l} \to -\infty$.

By selecting specific scale values (*e.g.* different in lengthwise and radial directions) the nonlinear system of Equations (2.6)–(2.7) transforms into a nondimensional form in which all the coefficients are equal to 1, and the only governing parameter, *i.e.*, nondimensional injection rate, is $\bar{\dot{q}}_n = \dfrac{2\mathrm{Eu}}{\pi c_{x0}} \dfrac{Q_n}{Vd^2}$, where d is the cavitator diameter.

A comprehensive numerical analysis has been performed, covering a cavity pulsation range from a single- to a ten-wave mode under different types of injection. The results of the analysis are in good qualitative agreement with known experimental data and the above linear theory.

An example of results of a multi-wave ($N \approx 6$) analysis is presented in Figure 11, $\bar{\dot{q}}_n = 10$. The oscillations are not strictly regular and feature variations in the pressure pulse and the number of waves, (also observed in experiments) due to the excitation of unstable lower eigenvalues. A phase trajectory $(\Delta\bar{p}', \Delta\bar{p})$ is of the converging (stable) spiral type, with instant energy supply at the moment of bubble detachment as in a pendulum clock.

Note that the most important result is that the accepted theoretical model reflects deep inherent properties of real cavities. Thus, the analysis shows that under growth of the injection rate, there exist switches between pulsation modes towards a greater number of waves along the cavity; this is also observed in experiments. This is especially pronounced for the following analysis conditions: under a continuous, or very slow change in the injection rate and in the absence of external disturbances, there is a critical injection rate value $\bar{\dot{q}}_n = 3{\cdot}26$ at which single-wave oscillations $R\,1$ spontaneously turn into two-wave ones $R\,2$ (see Figure 12). Hereafter N is the number of waves along the cavity, and RN denotes the corresponding mode.

Multi-wave transitions under change of injection rate are not that explicit. The multi-wave modes themselves are unstable. Both their parameters (cavity length, pulsation frequency,

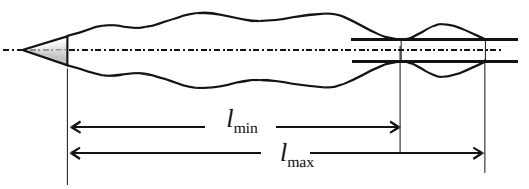

Figure 10. Gas-bubble detachment in the process of cavity pulsation.

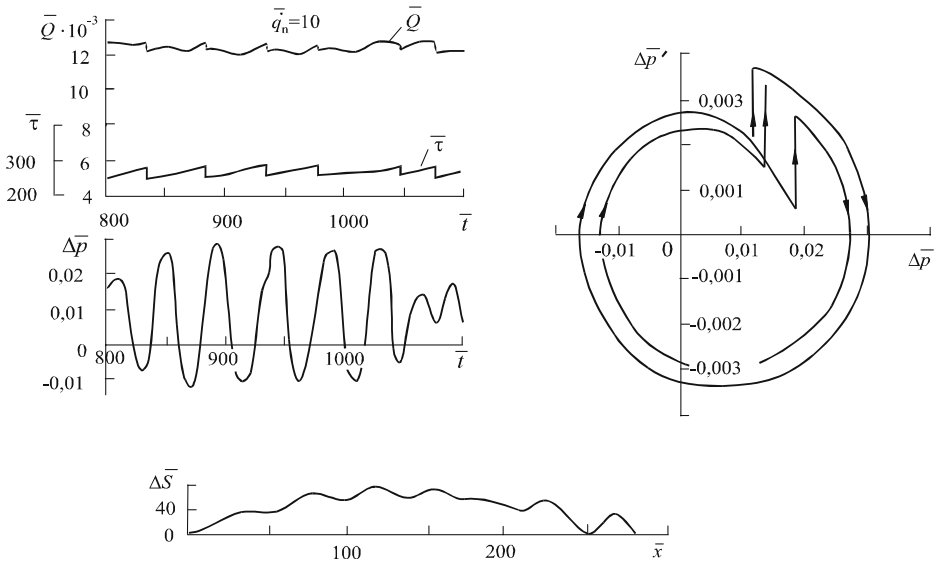

Figure 11. Multi-wave cavity-pulsation mode.

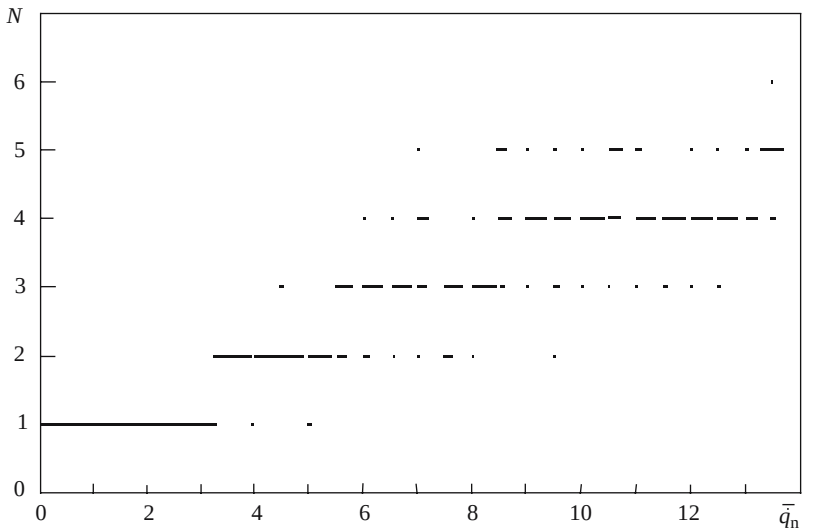

Figure 12. Change of cavity-pulsation modes with variation of the dimensionless gas-injection rate.

bubble volume), and number of waves N are unstable. Along with the main mode, there are cavities with a lower or higher number of waves.

Figure 12 shows the distribution of various pulsation modes RN as a function of the nondimensional injection rate $\bar{q}_n \leq 13{\cdot}75$. Cavities with different numbers of waves may occur at the same injection rate being kept for rather a long time ($\sim$ 20–30 periods of pulsation). The rate of occurrence of a given cavity mode as a percentage is displayed by the lengths of horizontal lines (100% relates to $\Delta\bar{q}_n = 0{\cdot}5$). One can see that generally the mode number N increases for increasing of injection rates. Approximate boundaries between modes can be indicated: transition from $R2$ to $R3$ occurs at $\bar{q}_n \approx 5{\cdot}5$; from $R3$ to $R4$ at $\bar{q}_n \approx 8{\cdot}5$; from $R4$ to $R5$ at $\bar{q}_n \approx 13{\cdot}3$.

3. Impact and immersion of a cylinder through a cylindrical liquid surface

3.1. Problem formulation

In an unbounded, incompressible, weightless, ideal liquid there exists a circular cavity of radius R, narrowing or expanding with a velocity $V_R(t)$ (the positive direction is towards the centre). A circular expanding body with radius $r < R$ (Figure 13), with a gap $\varepsilon = R - r$ is immersed symmetrically in the fluid with a variable velocity $V_y(t)$. The velocity of expansion of the cylinder is $V_r(t)$, the positive direction being out from the centre. Generally, relative radial motion is governed by the sum of the velocities $\tilde{V}_R = V_R + V_r$. It is shown in [34] that taking additional account for cavity and cylinder expanding results in the same formulas as those in [32, 33], with substitution of V_R by $\tilde{V}_R$.

To solve the problem, we shall use the well-known approach developed by Wagner for the immersion of an obtuse wedge [2]. Due to a small deadrise angle, the boundary conditions on the wedge and the free surface may be transferred to the undisturbed liquid surface. As a result, the immersion of an obtuse angle can be treated as an impact of a flat expanding plate on the surface of the fluid. At each instant of time the plate has a wetted width identical to that of the wedge. The velocity potential induced by the plate impact is used to determine the wedge wetted width by writing down an integral equation for the "meeting" of a liquid particle on the water surface with the wedge facet. The method is less reliable at higher deadrise angles, hence a nonlinear approach is needed.

Similarly, it is assumed in this case that the flow developing in the process of immersion of an expanding circle in a circular cavity is equivalent to the flow initiated by the impact of a circular arc of radius $r = R$. The difference from the plate impact is that the arc has two impact velocities: translational V_y and radial $\tilde{V}_R$. At each instant of time the width of the arc is assumed to be equal to the wetted width of the submerged circle (Figure 13, where $2B$ is the angle of the wetted surface). Then the velocity potential induced after combined impact of the arc is determined, and the integral equation of "meeting" is written down and solved.

Basically, Wagner's approach is valid for any ratio between cylinder and cavity radii; however, the cylinder immersion should be small, when the shapes of the submerged part and the free surface slightly deviate from the undisturbed circular liquid surface (when they produce a small angle with respect to this boundary). The solution becomes less accurate at greater immersion as well as at greater deadrise angle.

The accuracy of the solution depends on the gap ε, or radii ratio R/r. The smaller the gap, the closer is the circle to the cavity boundary, and the greater is the wetted width $2B$ within which the boundary conditions can be transferred onto an undisturbed cavity boundary. Thus, if $\varepsilon \to 0$, this is valid for the entire cylinder surface: $B \to \pi$ (see (3.7) below, η is the cylinder submersion). For a flat water surface ($\varepsilon \to \infty$, $R/r \to \infty$), the circular arc deviates greatly from the plane, even at small $2B$ angle, and the solution becomes inaccurate. Moreover, unlike for the infinite wedge, the above method based on a "meeting" integral equation is not meaningful for $B = \pi/2$ ($\eta/r = 0{\cdot}36338$) when the water surface rises to the horizontal diameter of the cylinder.

3.2. Oblique impact of an arc

Compared with [32, 33], the present paper concerns the impact problem in a more general formulation as a problem of an oblique impact (Figure 14). Consider an arc of radius R with central angle $2B$ striking the cylindrical fluid surface. The impact velocity $\vec{V}$ makes an angle

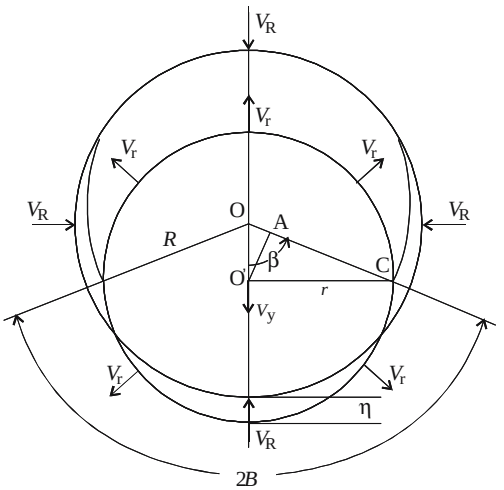

Figure 13. Immersion of a cylinder through a cavity boundary.

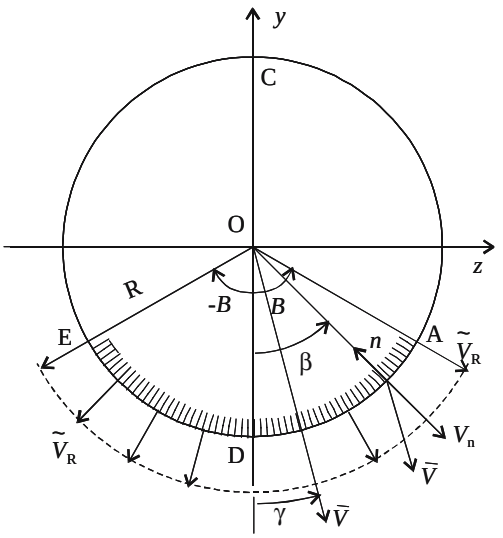

Figure 14. An oblique impact of a circular arc against a cavity surface.

γ with the arc symmetry axis, and the expansion velocity $\tilde{V}_R$ is directed along the radius at each point. On the free surface the potential is $\Phi = 0$.

Thus, we get an external boundary-value problem of mixed type, which is solved by use of Keldysh-Sedov's theorem [39, pp. 284–289]. The problem solution gives the velocity potential on the arc ($|\beta| \le B$):

$$\Phi = -2R\left(V_z \sin\frac{\beta}{2}\sqrt{a} + V_y\sqrt{a}\cos\frac{\beta}{2} - \frac{\tilde{V}_R}{2}\ \ln\ \frac{\cos\beta/2 - \sqrt{a}}{\cos\beta/2 + \sqrt{a}}\right), \tag{3.1}$$

and the normal velocity on the free surface ($|\beta| > B$):

$$V_n = V_z\left(-\sin\beta \pm \cos\frac{\beta}{2}\,\frac{\sin^2\beta/2 - a}{\sqrt{-a}}\right) + V_y\left(-\cos\beta \pm \sin\frac{\beta}{2}\,\frac{\cos^2\beta/2 + a}{\sqrt{-a}}\right)$$
$$+\tilde{V}_R\left(-1 \pm \frac{\sin\beta/2}{\sqrt{-a}}\right). \tag{3.2}$$

Here $V_z = V\sin\gamma$, $V_y = V\cos\gamma$, $a = \cos^2\beta/2 - \cos^2 B/2$. The plus and minus signs must be chosen on the intervals $B < \beta < \pi$ and $-\pi < \beta < -B$, respectively.

For vertical impact and expansion, the impulsive force P_y acting on the arc is directed along the Y-axis and can be determined from the expression

$$P_y = -2\rho R\int_0^B \Phi(\beta)\cos\beta\,d\beta = \rho\pi R^2\sin^2 B/2\left[\left(1+\cos^2 B/2\right)V_y + 2\tilde{V}_R\right]. \tag{3.3}$$

Similarly, the impulsive force acting on the arc at oblique impact is

$$P_z = -2\rho R\int_0^B \Phi(\beta)\sin\beta\,d\beta = \rho\pi R^2 V_z\sin^4 B/2. \tag{3.4}$$

Notice an interesting feature of an oblique impact. Let $\tilde{V}_R = 0$. We can find an angle γ_1 between the vertical axis and the impulsive force vector $\vec{P}$. From (3.3) and (3.4) we obtain

$$\tan\gamma_1 = \frac{P_z}{P_y} = \tan\gamma\,\frac{\sin^2 B/2}{1+\cos^2 B/2},$$

i.e., the directions of the impulsive force and the impact velocity do not coincide (vector "refraction").

From (3.3) and (3.4) we can determine the apparent masses of the fluid for side impact, vertical impact and expansion of the arc:

$$m_z^* = \rho\pi R^2 \sin^4 B/2, \quad m_y^* = \rho\pi R^2\left(1-\cos^4 B/2\right), \quad m_R^* = \rho\pi R^2\cdot 2\sin^2 B/2. \tag{3.5}$$

Applying the obtained results, we can determine approximately the hydrodynamic coefficients of the transversal forces:

$$C_y^{\alpha_y} = 2\sin^2 B/2(1+\cos^2 B/2), \quad \alpha_y = V_y/W, \quad C_y^{\alpha_R} = 4\sin^2 B/2, \quad \alpha_R = \tilde{V}_R/W,$$
$$C_z^{\psi} = 2\sin^4 B/2, \quad \psi = V_z/W.$$

Here W is the planing speed.

3.3. Symmetrical immersion of an expanding cylinder

The problem of symmetric immersion of a cylinder through a narrowing cavity boundary is solved in [32, 33]. Additional cylinder and cavity expansion are taken into account in [34]. The formulas that were derived coincide if the narrowing velocity V_R is substituted by the generalized velocity $\tilde{V}_R$.

We shall not repeat here the derivation of the integral equation for the liquid particle/cylinder contour "meeting" [32, 33]; written below is just the final formula for the equation:

$$2\eta - u(\varepsilon+\eta) = \frac{2}{\pi}\int_0^u \frac{r-\sqrt{r^2-(\varepsilon+\eta)^2 f(2-f)}}{\sqrt{f(u-f)}}\,\mathrm{d}f, \tag{3.6}$$

where $u = 1-\cos B$.

Equation (3.6) defines the relationship between the submergence η, the gap ε and the wetted width $2B$. This equation was obtained under the assumption of arbitrary variable velocities V_y, V_R and V_r, and from the point of view of Wagner's formulation it is valid for arbitrary gap and rather small submergence. In [32, 33], calculation of the wetted width for arbitrary gap is reduced to solving a transcendental equation.

Here the case for a small gap ($\varepsilon \ll r$) and a small submergence ($\eta \ll r$) is considered, when the right-hand side of (3.6) is zero to lowest order compared to the left-hand side. As a result, Equation (3.6) goes over into an equality

$$\cos B = \frac{\varepsilon-\eta}{\varepsilon+\eta} \quad \text{or} \quad \tan^2\frac{B}{2} = \frac{\eta}{\varepsilon}. \tag{3.7}$$

Substituting B from (3.7) in (3.5), we obtain the apparent masses

$$m_y^* = \rho\pi r^2\frac{2\varepsilon+\eta}{(\varepsilon+\eta)^2}\eta, \quad m_R^* = \rho\pi r^2\frac{2\eta}{\varepsilon+\eta}. \tag{3.8}$$

The vertical momentum of the liquid layer of unit thickness is

$$P_y = m_y^* V_y + m_R^*\tilde{V}_R.$$

The time derivative of the momentum is the force acting on the cylinder

$$f = \frac{\mathrm{d}}{\mathrm{d}t}\left(m_y^* V_y + m_R^* \tilde{V}_R\right) = \frac{\rho\pi r^2}{\varepsilon+\eta}\left[2\left(\frac{\varepsilon}{\varepsilon+\eta}V_y + \tilde{V}_R\right)^2 + \eta\left(\frac{2\varepsilon+\eta}{\varepsilon+\eta}\frac{\mathrm{d}V_y}{\mathrm{d}t} + 2\frac{\mathrm{d}\tilde{V}_R}{\mathrm{d}t}\right)\right]. \quad (3.9)$$

There are two limitations related to the use of Equation (3.9). The first is for the case of the cylinder leaving the liquid (negative velocities V_y or $\tilde{V}_R$). The second concerns the case of decelerated submergence (negative acceleration $\dot{V}_y$, $\dot{\tilde{V}}_R$). Closer consideration shows [34] that the necessary conditions for the existence of the force f are

$$\frac{\varepsilon}{\varepsilon+\eta}V_y + \tilde{V}_R > 0, \quad f > 0. \quad (3.10)$$

4. Model of cavity closure onto a jet

The Efros model with a re-entrant jet is shown in Figure 15. According to the classical Efros method, a cavity may be closed onto a solid body, or a central liquid jet of high intensity with the formation of circular re-entrant jet (*e.g.* Figure 16). The flow pattern here is similar to that of Efros' model.

Below a model of cavity closure onto a central liquid or incompressible gas jet is described and its approximate analysis given, the model being in some respects opposite to that of Efros. A circular re-entrant jet formed from a central jet is considered in this model instead of a re-entrant jet formed from an external flow as in Efros' model.

4.1. Physical model

Gravity is neglected; the flow is axisymmetric; all liquids are ideal and incompressible. Consider a cavity which closes onto a central jet of incompressible gas or liquid, with no total pressure loss in the jet and its branches. Like in the Efros model, the flow is potential, although there exist surfaces between external flow and gas (vapour) in the cavity with tangential velocity discontinuity. The flow pattern at the cavity tail may be described on the basis of the following considerations.

Just after the cavitator, the cavity is getting wider, then reaches a maximum diameter, upon which it is getting narrower, down to zero diameter at the closure. This narrowing in the tail affects the jet, making it slower and causing a pressure increase at the cavity boundary. By regarding the velocity field in the system of coordinates as linked with the undisturbed outer fluid, we can consider a velocity (energy) for the narrowing process. Depending on the relation between the energy of the jet and that of the narrowing, two possible cases can be realized: (1) The inward radial velocity on the cavity boundary is not totally eliminated; thus

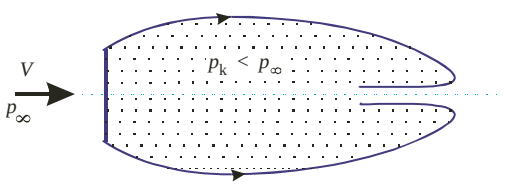

Figure 15. Classical Efros model of cavity closure with a re-entrant jet.

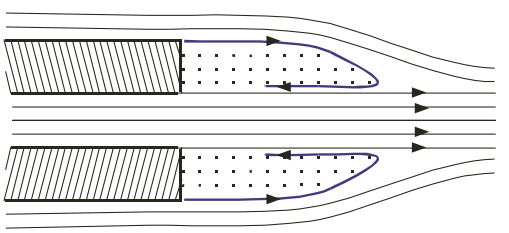

Figure 16. The Efros model with closure onto a central jet (a cavity produced by flow separation from a blunt afterbody is shown).

the cavity boundaries close onto each other with some finite speed. This case is closely related to the classical Efros model; (2) The radial cavity velocity is totally eliminated on the central jet; the cavity boundaries are not closed; a central jet exits the cavity.

Details of the latter flow pattern depend on the relationship between the jet stagnation pressure, p_0, and that of the surrounding flow, p_{0f}.

If $p_0 > p_{0f}$, Efros' closure onto a liquid jet is realized, as in Figure 17 or Figure 16 ($p_0 \gg p_{0f}$).

If $p_0 < p_{0f}$ (Figure 18), then in the region of jet-cavity interaction, critical points occur in the jet with pressure p_0. The points form a circle on the cavity boundary. The circle separates two branches of the initial central jet, *i.e.*, the part going out from the cavity, and the annular re-entrant jet. The latter is an important feature of this flow type, since if the central jet contains gas, it partially contributes to cavity ventilation.

4.2. Flow with central jet for $p_0 < p_{0f}$

A qualitative picture of the pressure distribution along the cavity-liquid boundary is shown in Figure 19. In the front part, the pressure is almost constant, and equals p_k. Then it increases and reaches its maximum value, the jet stagnation pressure p_0, at the line of critical points O. Then it decreases to the free-stream pressure at infinity, p_∞.

For further consideration, we shall replace this pressure curve with a step-function (dashed line in Figure 19). The central step height is p_0; initially, the coordinates of the front and rear edges of the step-function x_1, x_2 are unknown. They are associated with the times t_1, t_2 and the areas S_1, S_2, which are also unknown. Here also: S_c is the cross-sectional area of the undisturbed central jet, S_2 is the cross-sectional area of the jet downstream of the cavity, and S_3 is the cross-sectional area of the annular re-entrant jet.

Consider the cavity closure area more in details. The central jet is assumed to be slender enough, so that the jet-cavity interaction region, *i.e.*, the $x_2 - x_1$ interval is at the cavity tail. It allows for an assumption that the cavity-collapse velocity at x_1 is approximately equal, but opposite in sign, to the cavity-expansion velocity at the cavitator trailing edge: $\dot{S}(x_1) \approx -S_0' V$, where $V = \text{const}$ is the external-flow velocity. Starting from x_1, the cavity acquires a curvature of opposite sign under a positive pressure difference $p_0 - p_\infty > 0$ (local cavitation number $\sigma < 0$) and has approximately zero velocity $\dot{S}(x_2) \approx 0$ at x_2.

Let us apply the equation for the cavity cross-section expansion (2.1) to the $x_2 - x_1$ interval. Then two equations can be given: for the cavity-collapse velocity and for the cross-section areas, respectively (ρ is water density):

$$-S_0' V - \frac{k}{\rho}\int_{t_1}^{t_2} (p_\infty - p_0)\mathrm{d}v = \dot{S}(x_2) = 0, \quad S_1 - S_0' V(t_2 - t_1) - \frac{k}{\rho}\int_{t_1}^{t_2}\int_{t_1}^{u} (p_\infty - p_0)\mathrm{d}v\mathrm{d}u = S_2.$$

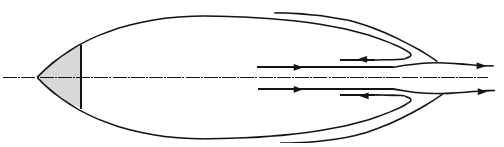

Figure 17. Efros' cavity closure onto a central jet; $p_0 > p_{0f}$.

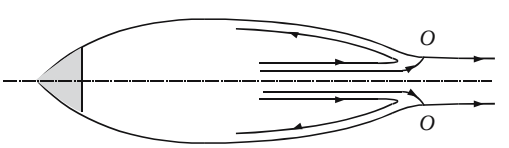

Figure 18. A proposed model of the closure onto a central jet; $p_0 < p_{0f}$.

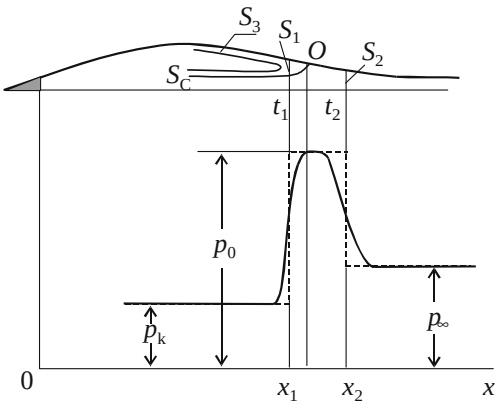

Figure 19. Pressure distribution at the cavity boundary.

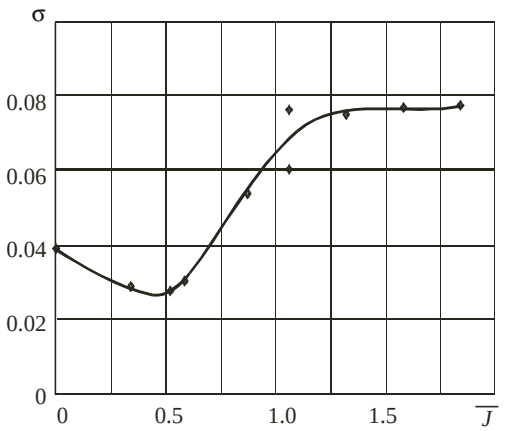

Figure 20. Experimental data on variation of cavity number σ with variation of the dimensionless jet momentum $\bar{J}$.

After calculating the integrals, we find $S_1 - S_2 = \dfrac{\rho V^2 S_0'^2}{2k(p_0 - p_\infty)}$. Using certain expressions from [40], namely $S_0' = \dfrac{2\pi\, R_n c_{x0}}{a}$, $k = \dfrac{4\pi\, c_{x0}}{a^2}$, where $a(\sigma) \approx \text{const}$, we have

$$S_1 - S_2 = \frac{\rho V^2 \pi\, R_n^2 c_{x0}}{2(p_0 - p_\infty)} = \frac{W_c}{p_0 - p_\infty}, \tag{4.1}$$

where W_c is the cavitator drag.

Now Equation (4.1), together with the equations for momentum,

$$\rho_0(S_2 V_2^2 - S_c\, V_0^2 - S_3 V_3^2) = p_k S_1 - p_0(S_1 - S_2) - p_\infty S_2, \tag{4.2}$$

continuity

$$S_c V_0 = S_2 V_2 + S_3 V_0, \tag{4.3}$$

and Bernoulli's equation

$$p_0 = p_k + \frac{1}{2}\rho_0 V_0^2 = p_\infty + \frac{1}{2}\rho_0 V_2^2 \tag{4.4}$$

can be applied to the total configuration shown in Figure 19. In these equations: $\rho_0 = \text{const}$ is the gas (liquid) density in the jet, V_0 is the velocity of the undisturbed jet, V_2 is the velocity of the jet downstream of the cavity, $V_3 = V_0$ is the re-entrant jet velocity. The total dynamic pressure of the external flow is $p_{0f} = p_\infty + \frac{1}{2}\rho\, V^2$.

Denoting $\dfrac{p_{0f}}{p_0} \approx \dfrac{\rho\, V^2}{\rho_0 V_0^2} = M > 1$, and assuming small cavitation number: $\sigma = \dfrac{2(p_\infty - p_k)}{\rho\, V^2} \ll 1$, we can take $\sigma\, M = o\,(1)$. Then from (4.4) we get:

$$V_2^2 = V_0^2(1 - \sigma\, M), \quad V_2 \approx V_0\left(1 - \frac{\sigma\, M}{2}\right).$$

Volume-per-second rates through the S_2 and S_3 sections are derived from (4.1) to (4.3):

$$q_2 = S_2 V_2 = S_c V_0 - \frac{W_c}{2\rho_0 V_0}(1 + \sigma\, M), \quad q_3 = S_3 V_0 = \frac{W_c}{2\rho_0 V_0}(1 + \sigma\, M), \tag{4.5}$$

and $q_0 = S_c V_0$ is total jet volume rate.

Let us denote $J = \rho_0 V_0^2 S_c$ as the momentum of the part of the jet passing through a cross-section per second. Let $\bar{J} = J/W_c$ be the dimensionless momentum. The small value σM may be neglected as compared to 1, whence the dimensionless form of (4.5) gives:

$$\bar{q}_2 = \frac{q_2}{q_0} = 1 - \frac{1}{2\bar{J}}, \quad \bar{q}_3 = \frac{1}{2\bar{J}}. \tag{4.6}$$

We see at once from (4.6) that the jet past the cavity ($q_2 > 0$) exists only if $\bar{J} > 1/2$. Thus, flow patterns are very different for $\bar{J} < 1/2$ and $\bar{J} > 1/2$. In the first case, there is no jet beyond the cavity, so the jet totally returns into it.

If $\bar{J} > 1/2$, the jet is divided into two parts: the re-entrant jet returns a mass-flow-rate portion $\bar{q}_3$; the mass portion to leave the cavity is $\bar{q}_2$. The greater the momentum, $\bar{J}$, the less is the returning part, and the greater is that which leaves.

These processes affect the cavitation number. When $\bar{J} = 0$, there is a free cavity with cavitation number σ. An increase of momentum in the range $0 < \bar{J} \leq 1/2$ leads to a greater re-entrant jet and a lower cavitation number as the re-entrant jet contributes to cavity ventilation.

If $\bar{J} > 1/2$, there is gas withdrawal from the cavity that increases with increasing $\bar{J}$, together with a growth of the cavitation number (compare the above peculiarities of the cavitation-number variation with the test results (Figure 20); the cavitation number reaches a minimum at $\bar{J} \approx 0{\cdot}5$ in experiment).

Table 1. Nomenclature

$a(\sigma) \approx$ const		S	cavity cross-sectional area
$\bar{A}$	complex amplitude of cavity disturbance	S_0	cavitator cross-sectional area $S_0 = \pi R_n^2$
b	amplitude-frequency response function	S_1	cavity cross-sectional area at x_1
$\bar{B}$	complex amplitude of forced pressure oscillations in a cavity	S_2	the cross-sectional area of the jet downstream of the cavity
$2B$	central angle of the wetted surface	S_3	the cross-sectional area of the annular re-entrant jet
c_{x0}	cavitator drag coefficient	S_c	the cross-sectional area of the central jet
C	the constant of the gas state equation	S_0'	initial rate of cavity expansion
$C_y^{\alpha_y}, C_y^{\alpha_R}, C_z^{\psi}$	hydrodynamic coefficients of transversal forces	S_T	the cross-sectional area of a body inside the cavity
d	diameter of cavitator	t	time
Eu	Euler number $\mathrm{Eu} = 2p_\infty / \rho V^2$	t_h	the time moment when cavitator passes through coordinate h
f	force acting per unit length of the cylinder	$t_1 = x_1/V, t_2 = x_2/V$	
f_1, f_2	cavity expansion equation coefficients	T	time scale
Fr	Froude number $\mathrm{Fr} = V/\sqrt{gd}$	V	external flow velocity
h	coordinate of a cavity cross-section	V_0	jet velocity
h_3	the coordinate of the section in which the cavity is closed	V_2	the velocity of the jet downstream of the cavity
H	the cavity inception coordinate	V_3	the re-entrant jet velocity $V_3 = V_0$
i	imaginary unit $\mathrm{i} = \sqrt{-1}$	$\vec{V}, V_z, V_y$	impact velocity and its components
j	serial number of an eigenvalue of the characteristic equation $j = 1, 2, \ldots$	V_n	the normal velocity of the fluid on the free surface
J	the momentum of the part of the jet passing through a cross section within a second $J = \rho_0 V_0^2 S_c$	V_r	velocity of circle expanding
		V_R	velocity of cavity narrowing/expanding
k	a coefficient of cavity expansion equation	$\tilde{V}_R = V_R + V_r$	
l	cavity length	W	planing speed

Table 1. Continued

l_0	cavity steady or averaged length value	W_c	cavitator drag
l_b	wavelength of the waves on the cavity surface	x	the distance between the cavitator and the given cross-section
$\dot{m}_n$, $\dot{m}_y$	mass rates per second for gas injection and loss	x_1, x_2	coordinates of the beginning and the end of a portion of the cavity with pressure p_0
m_z^*, m_y^*, m_R^*	apparent masses	α	damping coefficient in the equation of cavity oscillation
$M = p_{0f}/p_0$		α_{kp}	damping coefficient corresponding to the cavity stability boundary
$1/n$	polytropic factor	$\alpha_y = V_y/W$	
N	the number of waves along the length of the cavity	$\alpha_R = \tilde{V}_R/W$	
p_∞	pressure at infinity	γ	angle between the vertical axis and the impact velocity $\vec{V}$
p_v, p_k	vapour and gas pressure in a cavity	γ_1	angle between the vertical axis and the impulsive force vector $\vec{P}$
p_{k0}	steady (averaged) gas pressure in the cavity	ε	gap $\varepsilon = R - r$
$\Delta p = p_\infty - p_v - p_k \approx p_\infty - p_k$		η	depth of cylinder immersion
p_0	jet stagnation pressure	κ	jet ejection coefficient $\kappa = 0{\cdot}155$
p_{0f}	stagnation pressure of the surrounding flow	λ	complex eigenvalue of the characteristic equation $\lambda = \mu \pm i\omega$
$\vec{P}$, P_z, P_y	impulsive force and its components	μ	real part of an eigenvalue
q	external additional volume to disturb a cavity	ρ	fluid density
q_0	total jet volume rate $q_0 = S_c V_0$	ρ_0	jet density
q_2, q_3	volume per second rates through S_2 and S_3 sections	ρ_k	gas density in the cavity
$\bar{\dot{q}}_n$	the governing parameter of the nonlinear problem – nondimensional injection rate	σ	cavitation number $\sigma = 2\Delta p/\rho V^2$
		τ	time lag
Q	gas volume in a cavity	τ_0	steady value of τ
Q_0	steady (averaged) value of gas volume in a cavity	$\bar{\tau}_0$	the governing parameter of a linear problem – a dimensionless time lag
Q_n, Q_y	volume per second rate of gas injection and withdrawal from a cavity	φ	phase frequency response function
r	radius of circle expanding	Φ	velocity potential
R	radius of cavity narrowing or expanding	$\chi = \bar{\omega}\bar{\tau}_0/2$	
R_0	radius of the jet	$\psi = V_z/W$	
R_n	radius of cavitator	ω	imaginary part of an eigenvalue $\approx$ circular frequency of oscillations
RN	pulsation mode featuring N waves along the cavity		

a horizontal bar above a symbol means that the symbol is dimensionless
an overdotted symbol means the derivative with respect to time
an upper accent means a derivative with respect to other variables
a lower subscript j means correspondence to a jth eigenvalue

5. Conclusions

Three problems in high-speed hydrodynamics and supercavitation have been considered in this paper:

– Theoretical studies of the dynamic properties of slender ventilated cavities have been performed;

– A planar problem of the impact and immersion of an expanding cylinder into liquid with a cylindrical free surface of variable radius has been solved;
– A new theoretical model of cavity closure onto a gas jet has been proposed, and an approximate analysis of the model has been performed.

In the area of cavity dynamic properties (Section 2), the dynamic theory of slender axisymmetric cavities filled with a compressible gas has been developed. The key elements of the theory are:

– a closed problem formulation with gas mass balance in a cavity taken into account. The equation of cavity expansion for slender unsteady cavities has been used [19, 20, 40];
– a mathematical model of an unsteady cavity in the form of a system of nonlinear time-delay differential equations describing variations of cavity geometry and internal pressure has been developed;
– a linear theory of cavity stability and oscillations which unveils the nature and peculiarities of the phenomena has been considered. The theory is applicable to the main cavity types: cavities in a weightless liquid, vertical cavities in a gravity field, cavities with gas losses, cavities closed onto a gas jet, cavity undergoing forced oscillations;
– the generic property of ventilated cavities under various conditions is their oscillatory instability, which is at the basis of the known phenomenon of pulsation (self-oscillations) of cavities. The gas loss from the cavity is a damping factor;
– finding out the special role of a dimensionless parameter, *i.e.*, the dimensionless time lag, expressed eventually through a relation between Euler and cavitation numbers;
– a method to determine a total infinite set of complex eigenvalues of transcendental characteristic equations involving the extraction of a physically sensible dominating root;
– a detailed comparison of the obtained theory with experimental data on oscillations of axisymmetric and 2-D cavities;
– a qualitative analysis and numerical modeling of nonlinear cavity oscillations (self-oscillations) under variable gas injection with gas-bubble detachment taken into account.

Within the accuracy of constant parameter values, the above theory is totally valid for planar cavities also since the equation governing the expansion of a planar cavity has the same structure as that for axisymmetric cavities.

Basically, the mathematical model of an unsteady gas-filled cavity obtained here, the model being in the form of a system of nonlinear differential equations, makes it possible to consider a great many other problems of unsteady cavitation, *e.g.* forced cavity oscillations under different types of excitation, methods to control cavities, cavity dynamics under different mechanisms of gas loss, interaction between cavities and gas jets, etc.

In Section 3, a planar problem regarding the impact and immersion of an expanding cylinder into liquid with a cylindrical free surface of variable radius has been solved in Wagner's formulation.

A planar problem involving a symmetric and oblique impact of an expanding circular arc against a narrowing or expanding circular liquid boundary has been solved. The apparent masses of the fluid for side impact, vertical impact and for expansion of the arc and/or narrowing of the cavity have been determined. The hydrodynamic coefficients of the transversal forces have been determined approximately.

For immersion, only a symmetric problem was considered. Wagner's problem has been solved, and exact formulas have been derived for the solution assuming a small gap between the body and the cavity. The wetted width has been determined as a function of the gap and immersion depth. An approximate expression has been obtained for the hydrodynamic force acting per unit length of the cylinder, and conditions for the existence of this force have been

established. The force is determined within a shock problem formulation neglecting the second power of the fluid velocity.

It would be interesting to develop the solutions further in the two following areas:

– to solve Wagner's problem for an asymmetrical (oblique) immersion of a cylinder;
– to refine the expressions for the hydrodynamic force by taking into account the second power of the fluid velocity.

In Section 4, a cavity which closes onto a central jet of an incompressible gas or liquid, with no total pressure loss in the jet and its branches, was considered. The closure pattern with a re-entrant jet separating from the central one has been proposed.

The total dynamic pressure of the jet is assumed to be less than that of the surrounding flow. This causes critical points to occur in the jet within the area of jet/cavity interaction, the points making a circle on the cavity boundary. The circle separates a part of the initial central jet to turn this part into an annular re-entrant jet running back into the cavity. This is an important feature of this type of flow for, if the central jet contains gas, it partially contributes to cavity ventilation.

An approximate analysis of such a flow has been performed. The re-entrant jet flow rate has been determined as a function of the central jet momentum. The results of the analysis are in close agreement with experiment.

The proposed hydrodynamic flow pattern clearly explains the physical peculiarities of cavity closure onto a gas jet, and may be applied to examine experimental results and be used as a basic model for numerical codes.

Acknowledgements

The author greatly appreciates Prof. Alexander Korobkin (Lavrentyev Institute of Hydrodynamics, Novosibirsk, Russia), who has encouraged the author to write this paper and who has given further support in its preparation; also, the author greatly wishes to thank Prof. Vladimir Serebryakov (The Institute of Hydromechanics of NASU, Kiev, Ukraine) and Prof. Ivan Kirschner (Anteon Corporation, USA) for their general support and very useful discussions regarding the above topics. The author would like to thank all the reviewers who have thoroughly read the paper, and whose valuable comments have made it much better.

References

1. G.V. Logvinovich, *Hydrodynamics of Flows with Free Boundaries.* Kiev: Naukova Dumka (1969) 216 pp. (in Russian).
2. H. Wagner, Über Stoß- und Gleitvorgänge an der Oberfläche von Flüssigkeiten. *ZAMM* 4 (1932) 193–215.
3. G.E. Pavlenko, Fundamentals of the theory of planing. *Tr. NII GVF, Leningrad* 20 (1932) 23 pp. (in Russian).
4. D.A. Efros, Hydrodynamic theory of plane cavitating flow. *DAN SSSR, new series* 51 No 4 (1946) (in Russian).
5. M.P. Tulin, On an integrated cavitator-propulsor: the supercavitating pipe. In: G.G. Cherny, M.P. Tulin, A.G. Terentiev and V.V. Serebryakov (eds.), *Proc. of Int. Sci. School on High Speed Hydrodynamics*. Cheboksary, Russia/Washington, USA (2002) pp. 3–6.
6. N.E. Fine and J.S. Uhlman, Calculation of the added mass and damping forces on supercavitating bodies. In: G.G. Cherny, M.P. Tulin, A.G. Terentiev and V.V. Serebryakov (eds.), *Proc. of Int. Sci. School on High Speed Hydrodynamics*. Cheboksary, Russia/Washington, USA (2002) pp. 127–138.
7. Yu.D. Vlasenko, Experimental investigations of supercavitation flows at subsonic and transonic velocities. In: G.G. Cherny, M.P. Tulin, A.G. Terentiev and V.V. Serebryakov (eds.), *Proc. of Int. Sci. School on High Speed Hydrodynamics*. Cheboksary, Russia/Washington, USA (2002) pp. 197–204.

8. H. Braselmann, K.-H. Buerger and J. Koeberle, On the gas loss from ventilated supercavities – experimental investigation. In: G.G. Cherny, M.P. Tulin, A.G. Terentiev and V.V. Serebryakov (eds.), *Post-meeting v. of Int. Sci. School on High Speed Hydrodynamics*. Cheboksary, Russia/Washington, USA (2002) pp. 9–13.
9. I.N. Kirschner and L.G. Imas, Plume-supercavity interaction. In: G.G. Cherny, M.P. Tulin, A.G. Terentiev and V.V. Serebryakov (eds.), *Proc. of Int. Sci. School on High Speed Hydrodynamics*. Cheboksary, Russia/Washington, USA (2002) pp. 147–157.
10. X. Sheng, Y. Shu-Qun, Y. Kai and Ch. Jiu-Xi, Numerical simulation of a supersonic gas jet in liquid. In: G.G. Cherny, M.P. Tulin, A.G. Terentiev and V.V. Serebryakov (eds.), *Proc. of Int. Sci. School on High Speed Hydrodynamics*. Cheboksary, Russia/Washington, USA (2002) pp. 205–209.
11. Y. Tsujimoto and Yu.A. Semenov, New cavitation instabilities in turbomachineries: experimental observation and mathematical modeling. In: G.G. Cherny, M.P. Tulin, A.G. Terentiev and V.V. Serebryakov (eds.), *Proc. of Int. Sci. School on High Speed Hydrodynamics*. Cheboksary, Russia/Washington, USA (2002) pp. 29–39.
12. A.A. Rusetsky, Engineering application of separated cavitation flows in shipbuilding. In: G.G. Cherny, M.P. Tulin, A.G. Terentiev and V.V. Serebryakov (eds.), *Proc. of Int. Sci. School on High Speed Hydrodynamics*. Cheboksary, Russia/Washington, USA (2002) pp. 93–97.
13. A.S. Achkinadze, I.E. Stepanov, A. Berg and V.I. Krasilnikov, Numerical prediction of cavitation on propeller blades and rudder using the velocity based source panel method with modified trailing edge. In: G.G. Cherny, M.P. Tulin, A.G. Terentiev and V.V. Serebryakov (eds.), *Proc. of Int. Sci. School on High Speed Hydrodynamics*. Cheboksary, Russia/Washington, USA (2002) pp. 101–110.
14. I. Fedotkin and O. Yachno, Some problems of development of cavitation technologies for applications. In: G.G. Cherny, M.P. Tulin, A.G. Terentiev and V.V. Serebryakov (eds.), *Proc. of Int. Sci. School on High Speed Hydrodynamics*. Cheboksary, Russia/Washington, USA (2002) pp. 429–434.
15. G.H. Schnerr and W. Yuan, Unsteady cavitation in high speed injection nozzles. In: G.G. Cherny, M.P. Tulin, A.G. Terentiev and V.V. Serebryakov (eds.), *Proc. of Int. Sci. School on High Speed Hydrodynamics*. Cheboksary, Russia/Washington, USA (2002) pp. 369–376.
16. J.-M. Michel, Ventilated cavities: A contribution to the study of pulsation mechanism. In: L.I. Sedov and G.Yu. Stepanov (eds.), *Proc. of the IUTAM Symposium held in Leningrad*. Moscow: Nauka (1973) pp. 343–360.
17. E. Silberman and C.S. Song, Instability of ventilated cavities. *J. Ship Res.* 5 (1961) 13–33.
18. L.C. Woods, On the instability of ventilated cavities. *J. Fluid Mech.* 26 (1966) 437–457.
19. G.V. Logvinovich and V.V. Serebryakov, On methods of calculation of slender axisymmetric cavities shape. *Kiev: J. Hydromechanics* 32 (1975) 47–54 (in Russian.).
20. V.V. Serebryakov, Asymptotic approach for problems of axisymmetric supercavitation based on the slender body approximation. In: J.-M. Michel and H. Kato (eds.), *Proc. of Third Int. Symp. on Cavitation*, v. 2. Grenoble (1998) pp. 61–70.
21. E.V. Paryshev, The system of non-linear time-delay differential equations describing dynamics of unsteady axisymmetric cavities. *Tr. TsAGI* 1907 (1978) 3–16 (in Russian).
22. E.V. Paryshev, Theoretical investigation of stability and pulsation of axisymmetric cavities. *Tr. TsAGI* 1907 (1978) 17–40 (in Russian).
23. E.V. Paryshev, Oscillations of vertical cavities in ponderable liquids. *Uchenye Zapiski TsAGI* 3 (1981) 1–9 (in Russian).
24. E.V. Paryshev, Oscillations of vertical cavities in ponderable liquids. *Fluid Mech. Sov. Res*. 10 (1981) 122–133.
25. E.V. Paryshev, The principle of cavity expansion independence as a method of investigation of unsteady cavitation flows. *Tr. TsAGI* 2256 (1985) 43–50 (in Russian).
26. E.V. Paryshev, Numerical modeling of ventilated cavity oscillations. *Tr. TsAGI* 2272 (1985) 19–28 (in Russian).
27. E.V. Paryshev, Some issues related to analysis of unsteady cavitation flows. *Tr. TsAGI* 2644 (2003) 75–92 (in Russian).
28. E.V. Paryshev, Mathematical modeling of forced oscillations of a cavity filled with compressible gas. *Tr. TsAGI* 2644 (2003) 93–106 (in Russian).
29. E.V. Paryshev, The dynamic theory of supercavitation. In: G.G. Cherny, M.P. Tulin, A.G. Terentiev and V.V. Serebryakov (eds.), *Proc. of Int. Sci. School on High Speed Hydrodynamics*. Cheboksary, Russia/Washington, USA (2002) pp. 55–69.
30. G.V. Logvinovich, Some problems of planing. *Tr. TsAGI* 2052 (1980) 3–12 (in Russian).
31. G.V. Logvinovich, Problems of contemporary hydrodynamics. *Tr. TsAGI* 2256 (1985) 6–21 (in Russian).

32. A.D. Vasin and E.V. Paryshev, Immersion of a cylinder in a fluid through a cylindrical free surface. *Mekhanika Zhidkosti i Gasa* 2 (2001) 3–12 (in Russian).
33. A.D. Vasin and E.V. Paryshev, Immersion of a cylinder in a fluid through a cylindrical free surface. *Fluid Dynamics* 36 (2001) 169–177.
34. E.V. Paryshev, The plane problem of immersion of an expanding cylinder through a cylindrical free surface of variable radius. In: G.G. Cherny, M.P. Tulin, A.G. Terentiev and V.V. Serebryakov (eds), *Proc. of Int. Sci. School on High Speed Hydrodynamics*. Cheboksary, Russia/Washington, USA (2002) pp. 277–283.
35. M.I. Gurevich, *The Theory of Jets in an Ideal Fluid.* Moscow: Nauka (1979) 536 pp. (in Russian).
36. L.G. Guzevsky, Numerical analysis of cavity flows.*Preprint of Inst. of Thermophysics, Novosibirsk* 40–79 (1979) 36 pp. (in Russian).
37. R.N. Cox and W.A. Clayden, Air entrainment at the rear of a steady cavity. In: *Proc. of Symp. on naval hydrodynamics*. Teddington (1955).
38. L.A. Epshteyn, Determination of the amount of gas needed to maintain a cavity behind a body moving at low Fr number. *Tr. TsAGI* 824 (1961) 45–56 (in Russian).
39. M.A. Lavrentiev and B.V. Shabat, *Methods of the Theory of Functions of a Complex Variable.* Moscow: Nauka (1958) 678 pp. (in Russian).
40. G.V. Logvinovich, The issues on the theory of thin axisymmetric cavities. *Tr. TsAGI* 1797 (1976) 3–17 (in Russian).